

Binary Formation in Planetesimal Disks II. Planetesimals with Mass Spectrum

Junko D. KOMINAMI *

Earth-Life Science Institute, Tokyo Institute of Technology
kominami@mail.jmlab.jp

and

Junichiro MAKINO

RIKEN Advanced Institute for Computational Science
Earth-Life Science Institute, Tokyo Institute of Technology
makino@mail.jmlab.jp

(Received ; accepted)

Abstract

Many massive objects have been found in the outer region of the Solar system. How they were formed and evolved has not been well understood, although there have been intensive studies on accretion process of terrestrial planets. One of the mysteries is the existence of binary planetesimals with near-equal mass components and highly eccentric orbits. These binary planetesimals are quite different from the satellites observed in the asteroid belt region. The ratio of the Hill radius to the physical radius of the planetesimals is much larger for the outer region of the disk, compared to the inner region of the disk. The Hill radius increases with the semi major axis. Therefore, planetesimals in the outer region can form close and eccentric binaries, while those in the inner region would simply collide. In this paper, we carried out N -body simulations in different regions of the disk and studied if binaries form in the outer region of the disk. We found that large planetesimals tend to form binaries. A significant fraction of large planetesimals are components of the binaries. Planetesimals that become the components of binaries eventually collide with a third body, through three-body encounters. Thus, the existence of binaries can enhance the growth rate of planetesimals in the Trans-Neptunian Object (TNO) region.

Key words: planets and satellites: formation

* 2-12-1-IE-1 Ohokayama, Meguro-ku, Tokyo, 152-8550, Japan

1. Introduction

In the trans-Neptunian region, numerous planetesimal binaries have been found. So far, 79 planetesimal binaries have been found in the Trans-Neptunian object (TNO) region (<http://www.johnstonsarchive.net/astro/tnoslist.html>). This number is about $\sim 10\%$ of known TNOs between 30AU and 70AU (Stephens and Noll, 2006), and $\sim 30\%$ of the objects in the Cold Classical Kuiper Belt (Noll et al., 2008a).

Some asteroids in the main belt have satellites (e.g. Chapman et al. 1995). These satellites have relatively small mass compared to the primaries, and their eccentricities are quite small (Pravec et al. 2006). On the other hand, Trans-Neptunian binaries (TNBs) are known to have almost equal brightness (Noll et al. 2008b), implying comparable mass. Hence, planetesimal binary systems with mass ratio ~ 1 are frequently observed in the TNO region. The distribution of the eccentricities of TNBs is pretty wide, from ~ 0.1 to ~ 0.9 .

On the other hand, such systems have been hardly found in the asteroid belt region. The main physical difference between the inner region of the disk and the outer region of the disk is the ratio between the Hill radius and the physical radius of the planetesimals. Hill radius (r_h) of a planetesimal with mass m and semi major axis of a is given by $(m/3M_*)^{1/3}a$. Since it is proportional to a , it is 30 times larger at 30AU compared to that of 1AU for a same planetesimal. Hence, the way two planetesimals interact can be quite different in the TNO region and in the inner region, like the asteroid belt region. Some of the inner main belt objects are known to have relatively small size ratio (around 1:3) and small separation (Johnston 2012). They are most likely to be formed through the breakup of fast rotating asteroids (Walsh & Richardson 2006, Walsh et al. 2008, 2012). One almost equal-sized binary system, 90 Antiope, was found in 2000 (Merline et al. 2000). Its origin is so far not well understood, but a recent observation indicates that two components are chemically similar (Marchis et al. 2011), indicating the primordial origin of the binary.

Since the physical ratio of planetesimals in unit of the Hill radius are large in the inner region of the disk, two planetesimals can easily collide. Some of the collisions form fragments around planetesimals, resulting in small planetesimals orbiting around large planetesimal with small eccentricity. On the other hand, in the TNO region, Hill radii of the planetesimals are large. Therefore, physical collisions are less frequent, and complex interactions, including three-body encounters, are more frequent compared to the inner region. Large planetesimals tend to have smaller random velocities than those of small planetesimals due to the equipartition of the energy. Since the binaries are formed through three-body encounters, the eccentricity of the binaries is not restricted to small values.

Several formation scenarios have been proposed to explain the observed characteristics of TNBs (Weidenschilling 2002, Goldreich et al. 2002, Funato et al. 2004, Astakhov et al. 2005, Nesvorný et al. 2010). Weidenschilling (2002) proposed a scenario in which two planetes-

imals collide and accrete within the gravitational effect of the third body. However, collision frequency is too low to explain the number of observed TNBs. Goldreich et al. (2002) proposed two mechanisms. When the distance between two bodies becomes closer than the Hill radius, a third planetesimal encounters with them and takes away the energy leaving the two planetesimals being gravitationally bound (Goldreich et al. 2002). This is the scenario that we described above. Another mechanism Goldreich et al. (2002) proposed is that instead of the third planetesimal, swarm of small planetesimals takes away the energy of two encountering planetesimals (Goldreich et al. 2002). Exchange of a small satellite with another large planetesimal is proposed by Funato et al. (2004). Transitional binary being tightened by several close encounters of other planetesimals (Chaos-Assisted Capture) is proposed by Astackhov et al. (2005). Planetesimal binary formation by gravitational instability is introduced by Nesvorný et al. (2010).

All of these studies, except for Nesvorný et al., gave purely theoretical models. Nesvorný et al. performed the simulation of gravitational collapse of small planetesimals. Except for this work, no self-consistent numerical study of formation process of binaries in the TNO region is reported so far. Kominami et al. (2011) performed N -body simulation of disks of equal-mass planetesimals at 30 AU in order to see if the binary formation is a natural outcome in the TNO region. They systematically changed r_h/r_p (r_p being the physical radius), and the number density of planetesimals to study the effect of the binaries on the collision rate of planetesimals. They found that binaries are involved in $1/3 - 1/2$ of all collisions, and that the collision rate is increased by about a factor of a few compared to the theoretical estimate for the direct two-body collisions. In the terrestrial planet region, binaries are less important, because the ratio r_h/r_p is relatively small. Direct two-body collisions take place instead of binary formation. Although the duration of their simulations was short, they clearly demonstrated that the accretion process in the TNO region is different from that in the terrestrial planet region.

In the present paper, we report the result of N -body simulations with realistic mass distributions of planetesimals. We show which part of the mass spectrum is affected by the formation of the binaries. We found that the binary fraction of the massive planetesimals is high, and that a significant fraction of collisions between large planetesimals is through binary-single body interactions.

In Section 2, we explain the calculation method. Section 3 gives the results. We discuss the increase of the accretion rate due to the binary formation in section 4. The summary is given in section 5.

2. Calculation Model and Method

2.1. Initial Conditions

We consider the initial model which is consistent with the standard view of the collisional growth of the planetesimals. The distribution of planetesimal mass is a power-law and the random velocities of planetesimals are in the thermal equilibrium. We did not include the effect of the gas drag for simplicity. Also, we assumed the simple perfect accretion model. Thus, we effectively studied three-body formation, dynamical-friction model, chaos-assisted capture, but not models like Giant Impact or gravitational collapse.

Table 1 summarizes the initial conditions. In all runs, the initial models are narrow rings. We studied models with four different values of the initial semi-major axis (1,3,10 and 30). The mass distribution is given by

$$ndm \propto m^{-p}dm, \quad (1)$$

where n is the number density of planetesimal mass m . The power index p is about 2.5 after runaway growth (Kokubo and Ida 1996). Since the mass distribution of TNOs is not well understood, we adopt the above power index ($p = 2.5$) obtained in numerical simulations. The minimum and maximum mass, m_{\min} and m_{\max} , are $2 \times 10^{22}\text{g}$ and $2 \times 10^{24}\text{g}$, respectively. The values m_{\min} and m_{\max} have been fixed for simplicity. The observed TNOs are about ~ 100 km in size. In order to keep the simulations feasible, we constrained the number of planetesimals and hence have to keep the planetesimal mass large. From theoretical point of view, growth timescale and other behavior would be the same if physical quantities are properly scaled with the Hill radius. So we believe the relatively large mass used in our study does not cause serious problems. In order for the ring not to be too narrow, we set the planetesimals to be large as described. The number density used here is the value derived from the so-called minimum-mass solar nebula (Hayashi 1981). The eccentricity and inclination of planetesimals are given by the Maxwellian distribution. The initial RMS eccentricity of planetesimals is given by

$$\langle e^2 \rangle^{1/2} = \eta \left(\frac{m_{\max}}{3M_{\odot}} \right)^{1/3} \left(\frac{m}{m_{\max}} \right)^{-1/2}, \quad (2)$$

where η is a parameter. We varied η from 0.05 to 0.4 in order to study the effect of the initial velocity dispersion. For all models, we used $\langle e^2 \rangle^{1/2} = 2\langle i^2 \rangle^{1/2}$ (Ida and Makino, 1992). We create initial models so that there is no binary.

2.2. Orbital Integration

The equation of motion of a planetesimal is

$$\frac{dv_j}{dt} = -\frac{GM_{\odot}}{|r_j|^3}r_j - \sum_{k \neq j} \frac{Gm_j}{|r_j - r_k|^3}(r_j - r_k), \quad (3)$$

where r_j is the heliocentric position vector, v_j is the velocity vector, and m_j is the mass of

particle j , and G and M_\odot are the gravitational constant and the solar mass, respectively. The first and second terms are the gravity of the Sun and the mutual gravity between the particles, respectively. Since the total mass of the planetesimals is $\sim 10^{-6}M_\odot$, we neglect the indirect term. We use the 4th-order Hermite scheme (Makino and Aarseth 1992, Kokubo et al. 1998) using individual time step with block step algorithm for orbital integration. The energy error was monitored in the simulations. The error was within 10^{-6} level throughout the simulations. The mutual gravity term is calculated using GRAPE-DR (Makino et al. 2007). The integration time is 10^4 years. The number of binaries becomes roughly constant after several thousand years.

We take into account the particle accretion following the treatment in the previous works (e.g., Kokubo and Ida 1996, 1998). For simplicity, we use the perfect accretion model, in which we let two planetesimals merge when the distance between them becomes less than the sum of their radii. When the binary induced collisions take place, the relative velocity of the components can be high enough to produce some fragmentation. This effect has not been considered yet, and should be discussed in future study. The physical radius of a planetesimal is determined by its mass m and the density ρ as

$$R = \left(\frac{3}{4\pi} \frac{m}{\rho} \right)^{1/3}. \quad (4)$$

We assume $\rho = 3 \text{ g cm}^{-3}$. The solid density of the planetesimals in the TNO region is not well understood, and it might be more reasonable to use a smaller value. We adopted the typical density in the terrestrial region, which is not far from that of the observational value ($\sim 1 - 2 \text{ g cm}^{-3}$, e.g. Grundy et al. 2007, Johnston 2012).

2.3. Binary Definition

In this paper, we define a pair of planetesimals as binary, if their specific Jacobi energy E_J , defined as,

$$E_J = \frac{1}{2}(\dot{x}^2 + \dot{y}^2 + \dot{z}^2) - \frac{3}{2}\Omega_K^2 x^2 + \frac{1}{2}\Omega_K^2 z^2 - \frac{G(m_1 + m_2)}{r} + \frac{9}{2}r_H^2 \Omega_K^2, \quad (5)$$

under the Hill approximation (Nakazawa and Ida 1988), is negative, where x, y, z are relative cartesian coordinates of two planetesimals whose masses are m_1 and m_2 and Ω_K is the Kepler angular velocity at the barycenter given as $\sqrt{GM_\odot/a^3}$. When the distance between two planetesimals becomes smaller than the mutual Hill radius, r_H , we calculate E_J . The mutual Hill radius r_H of m_1 and m_2 is defined as

$$r_H = \left(\frac{m_1 + m_2}{3M_\odot} \right)^{1/3} \left(\frac{a_1 m_1 + a_2 m_2}{m_1 + m_2} \right), \quad (6)$$

where a_1 and a_2 are the semi major axes of m_1 and m_2 , respectively.

There are some pairs of which components orbit around each other but have positive E_J . However, the number of such pairs is negligible and they do not make substantial difference in

the results.

3. Results

3.1. Evolution of Velocity Dispersion

Figure 1 shows the evolution of the velocity dispersion for four runs: S30e0.05, S30e0.1, S30e0.2 and S30e0.4. The plot with $\eta = 0.05$ corresponds to the simulation result of S30e0.05, $\eta = 0.1$ corresponds to S30e0.1, $\eta = 0.2$ corresponds to S30e0.2 and $\eta = 0.4$ corresponds to S30e0.4. We can see that the velocity dispersion after 10^3 - 10^4 years is pretty similar for all runs. The velocity dispersion is almost flat for $m < 2 \times 10^{23}$ g, then approaches to the thermal equilibrium of $\langle e^2 \rangle \propto m^{-1}$ for larger mass. Figure 2 shows the time evolution of the mean eccentricities for models S30e0.05, S30e0.10, S30e0.20 and S30e0.40. The mass range is divided into 5 bins with the same logarithmic width. The evolution of the eccentricity is quite similar for different mass bins after 100 - 1000 years, and reaches to similar values independent of initial values of η after 10^4 years. Note that since the number of the planetesimals in the largest mass bin is small, there are some fluctuations, especially when η is small. The velocity dispersion is far from the thermal equilibrium for the low-mass part. This is because the equipartition time scale is much longer than the heating time scale. On the other hand, the high-mass end ($m > 5 \times 10^{23}$ g) is approximately in the equipartition, which means massive planetesimals have smaller random velocity.

3.2. Evolution of Mass Distribution

Figure 3 shows the mass distributions at $t = 10^3, 10^4$ years and initial mass distribution for runs S30e0.10 and S30e0.20, which are the realistic models in the sense that initial velocity dispersion is fairly high. When we compare the long dashed curve and short dashed curve, it is clear that the number of planetesimals with mass greater than $\sim 2 \times 10^{24}$ g increases with time. As we will see in section 3.5, most of the collisions after 10^3 years are binary induced collisions.

3.3. Binary Formation Process

Figure 4 shows an example of the binary formation process in run S30e0.05. First, blue and red dots approach to each other, and experience a close encounter. After the encounter, the red body becomes weakly bound to the black one. Then third planetesimal (magenta) encounters with the red body and takes away some energy. As a result, the red body becomes bound to the black body. This formation process is the three-body process discussed in Goldreich et al. (2002). Figure 5 shows examples of the binary formation process. The dotted curves show the distance between the binary components and the solid curves show the semi major axis. The quantities are plotted when Jacobi energy is negative. In all of these cases, a third body is involved in the formation of the binary.

3.4. Mass Distribution of Binaries

Figure 6 shows the fraction of binary mass in each mass bin. The solid line corresponds to 10^2 years, long dashed line to 10^3 years and the short dashed line to 10^4 years. The difference is not so large, but if we compare the curves at 10^3 and 10^4 years, we can see that binary fraction shows some decrease in the low-mass side but essentially unchanged in the high-mass side. Figure 7 shows the time evolution of the number of binaries in runs S30e0.05, S30e0.1, S30e0.2 and S30e0.4. In the runs with small η , many binaries are formed initially, when the velocity dispersion is low. In the case of run with $\eta = 0.4$, the total number of binaries keeps increasing, even though the velocity dispersion is increasing slowly. Initial increase of the binaries is the effect of the initial condition. Binaries form more easily when the random velocities of the planetesimals are small. The increase in the random velocity is very large for models with low initial eccentricity. In these models many very soft binaries are initially formed, and most of them were destroyed after the random velocity increased. In figure 8, we can see that the large fraction of binary components are massive ($m > 5 \times 10^{22}$ g) at $t = 10^4$ years. At $t = 10^4$ years, $\sim 10\%$ of planetesimals in the highest mass bin are in binaries for all runs. This result shows that large planetesimals tend to form binaries, and once they are formed, they stay as binaries. In the runaway growth model, the behavior of the massive bodies determine the evolution. Since large planetesimals tend to form binaries, the accretion process can be significantly affected by the presence of binaries.

3.5. Number of Collisions

Although the number of collisions in the outer region is fewer than that in the inner region, a significant number of planetesimals experience collisions in runs S30e0.05, S30e0.10, S30e0.20 and S30e0.40. There are two types of collisions. The first is the ordinary collision which is of the same type of as what happens in the inner region. Another type of collision is the binary induced collision. First, two bodies become gravitationally bound through three-body interaction. Then a third body perturbs their orbits and one of the components collide with the third body or with the other component. The number of such collisions is 103 in S30e0.05, 71 in S30e0.10, 26 in S30e0.20 and 11 in S30e0.40.

In order to determine the type of a collision, we carried out the following procedure. We look at the snapshot $100/(2\pi)$ years before the collision. First we check the Jacobi energy of the colliding two bodies and see if it is negative. If so, we count them as a binary. If not, we look for the neighboring particles of the colliding particles. If we find a third body within the mutual Hill radius of the colliding particles, we calculate the Jacobi energy of the closest two bodies (one of the colliding two and the third body). If the Jacobi energy is negative, that collision is also counted as binary-induced collision. The Jacobi energy of the two particles is calculated using the position and the velocity vector. We checked if the colliding two bodies are really orbiting around each other at least several orbits.

Figure 9 shows the mass distribution of particles participated in collisions in runs S30e0.05, S30e0.10, S30e0.20 and S30e0.40. Solid and dashed curves indicate binary-induced and non-binary-induced collisions, respectively. The slope of the mass distribution of collided planetesimals is shallower than that of the initial mass distribution. Moreover, the slopes of the solid curves are somewhat shallower than that of the dashed curves, which means that the fraction of binary induced collisions over the total number of collisions is higher for larger planetesimals.

In figure 10, we show all collisions in runs S30e0.05, S30e0.10, S30e0.20 and S30e0.40 on the m_p - m_s plane, where m_p and m_s are the mass of particles collided ($m_p \geq m_s$). It is clear that binary-induced collisions have systematically larger values of m_s/m_p compared to non-binary-induced collisions. To see this tendency more quantitatively, we calculated average values of m_s/m_p for massive and less massive primaries.

The result is shown in figure 11. In the case of $\eta = 0.4$, m_s/m_p is higher for larger m_p in the case of binary-induced collisions, while it is lower for larger m_p in the case of non-binary-induced collisions. Though not this clear, similar tendency is visible for other values of η , except for $\eta = 0.05$ where the difference is small. Since the number of collisions is similar for two types of collisions, this difference in the average mass of the secondary means that the growth of the mass of massive bodies comes primarily from binary-induced collisions. In other words, massive planetesimals in the TNO region grow through binary-induced collisions, not through ordinary, non-binary induced collisions.

Figure 12 shows the mass fraction of the binary-induced collisions over total collisions, as the function of the primary mass. For runs with large η (0.2 and 0.4), we can see the tendency that the fraction of binary-induced collision is higher for larger m_p .

We can conclude that, for massive planetesimals, binary-induced collisions are frequent, and they are the main route of the growth of massive planetesimals.

4. Discussion

Here we estimate the collision probability increase due to the formation of planetesimal binaries. Let the binary induced collision probability to be $P_{c,bin}$, usual collision probability P and the total collision probability be $P_{total} = P_{c,bin} + P$. From Makino et al. (1998), usual collision probability of m and m' is

$$P = \frac{1}{\max(H, H')} \pi (r + r')^2 \left(1 + \frac{v_{esc}^2}{v_{rel}^2} \right) v_{rel} \quad (7)$$

where H is the scale height, r is the physical radius of mass m , $v_{esc} = \sqrt{2G(m + m')/(r + r')}$ is the escape velocity and $v_{rel}^2 = v^2 + v'^2$ is the relative velocity. The value v_{rel} can be written as $v_{rel} \sim ev_k = e\sqrt{G(m + m')/r_c}$, where $r_c = (mr + m'r')/(m + m')$ is r of the center of mass of m and m' . Hence, P can be written as

$$P = \frac{1}{\max(H, H')} \pi (r + r')^2 \left(1 + \frac{2}{e^2} \frac{mr + m'r'}{(r + r')(m + m')} \right) e \sqrt{\frac{G(m + m')^2}{mr + m'r'}} \quad (8)$$

On the other hand, binary induced collision probability $P_{\text{c,bin}}$ can be written as

$$P_{\text{c,bin}} = \frac{P_{\text{b}}}{\max(H, H')} \pi a_{\text{b}}^2 P_{\text{L3}} \left(1 + \frac{v_{\text{esc,b}}^2}{v_{\text{rel}}^2} \right) v_{\text{rel}} \quad (9)$$

where

$$v_{\text{esc,b}} = \sqrt{\frac{2G(m + m')}{a_{\text{b}}}} \quad (10)$$

and a_{b} is the typical semi major axis of binaries. We assume $a_{\text{b}} \sim r_{\text{H}}/10$. Here, P_{L3} is the probability of physical collision after a binary experienced close encounter with a third body. Eq.(9) can be written as

$$P_{\text{c,bin}} = \frac{P_{\text{b}}}{\max(H, H')} \pi a_{\text{b}}^2 P_{\text{L3}} \left(1 + \frac{2(mr + m'r')}{e^2 a_{\text{b}} (m + m')} \right) e \sqrt{\frac{G(m + m')^2}{mr + m'r'}}. \quad (11)$$

Hence, from (11) and (8) we obtain

$$\frac{P_{\text{c,bin}}}{P} = P_{\text{b}} \frac{a_{\text{b}}^2}{(r + r')^2} \left(\frac{1 + 2(mr + m'r')/(e^2 a_{\text{b}} (m + m'))}{1 + 2(mr + m'r')/(e^2 (r + r')(m + m'))} \right) P_{\text{L3}} \quad (12)$$

Let us assume $a_{\text{b}} \sim r_{\text{H}}/10$, $r_{\text{H}} \sim 100r$. Also, if we assume $1 \ll 2(mr + m'r')/(e^2 a_{\text{b}} (m + m'))$ and $1 \ll 2(mr + m'r')/(e^2 (r + r')(m + m'))$, eq(12) becomes

$$\frac{P_{\text{c,bin}}}{P} \sim P_{\text{b}} \frac{a_{\text{b}}^2}{(r + r')^2} \frac{r + r'}{a_{\text{b}}} P_{\text{L3}} \sim P_{\text{b}} P_{\text{L3}} \frac{a_{\text{b}}}{r + r'} \quad (13)$$

As shown in the previous section, When m is large, $P_{\text{b}} \sim 0.1$. If we assume $P_{\text{L3}} \sim 1$, we have

$$P_{\text{total}} = P_{\text{c,bin}} + P = (1 + P_{\text{b}} P_{\text{L3}} \frac{a_{\text{b}}}{r + r'}) P \sim P. \quad (14)$$

Thus, roughly speaking, the rate of binary-induced collision is comparable to that of non-binary induced collisions, in our model calculations. The enhancement of the growth rate due to the binary-induced collisions is larger for the following two reasons.

First, as discussed in section 3.4, the secondary mass is larger for the binary-induced collisions by a factor of three or around. This difference directly results in the increase of the growth rate by the same factor.

Second, in our simulations, the planetesimals tend to spread out radially, since the width of the initial planetesimal ring is still rather narrow (figure 13). The surface density in the radial range of 30.0 - 30.2 AU decreased by roughly a factor of two from the initial value (figure 14), and the “average” density by roughly a factor of three. Thus, the total non-binary-induced collision rate should have decreased by factor between five and ten (Goodman and Hut 1993). Therefore, the relative frequency of the binary-induced collision would be a few times higher than what is observed in our model, if the radial diffusion of planetesimals are suppressed.

5. Summary

We carried out N-body simulations of planetary growth in the outer region of the disk in order to study the effect of binaries. Planetesimals with realistic size distribution are considered. Our main findings are summarized as follows. Binaries are formed in the outer region of the disk. They are formed through three-body encounters. The random velocities of the planetesimals increase with time. Planetesimals with large mass tend to become binary components. The binaries collide through three-body encounters with third bodies. Compared to non-binary-induced collisions, binary-induced collisions prefer massive primaries and very strongly prefer massive secondaries. As a result, the growth of planetesimals happens mainly through binary-induced collisions. We estimate that growth timescale can be reduced by a factor of five to ten, due to the formation of binaries.

Since the initial planetesimal rings we used are narrow, the planetesimals tend to spread out radially and the density decreases from the initial value. The collision rate and the binary formation rate decrease as well. The actual number of the binary formation rate and binary-induced collision rate could be several times higher if the reduction of the surface density is prevented. Hence, the effect of the planetesimal binary formation onto the accretion rate of planetesimals should be significant in TNO region.

Timescale for the formation of Uranus and Neptune might be reduced by this factor, when in situ formation is assumed. The mechanism we propose will help us to understand the formation of outer planets and large TNOs.

Acknowledgment

Part of the results is obtained by using the K computer at the RIKEN Advanced Institute for Computational Science (Proposal number hpci130026). This work was supported in part by MEXT SPIRE Field 5 The origin of matter and the universe and JICFuS. J.K. thanks Hiroshi Daisaka for letting use his computer resources, fruitful discussion and encouragements. We thank the anonymous referee for the careful and detailed comments which helped us to improve the paper.

References

- Askatov S.A., A.L. Ernestine & D. Farrelly. 2005, MNRAS, 360, 401-415
- Chapman et al. 1995, Nature, 374, 783-785.
- Funato, Y., J. Makino, P. Hut, E. Kokubo & D. Kinoshita. 2004, Nature, 427, 518-520.
- Goldreich, P., Y. Lithwick & R. Sari. 2002, Nature, 420, 643-646.
- Grundy, W. M. et al. 2007, Icarus, 191, 286-297.
- Hayashi, C. 1981, Progress of Theoretical Physics Supplement, No. 70, pp. 35-53.
- Ida, S. & J. Makino. 1992. Icarus, 96, 107-120.
- Johnston, W. R. 2012. NASA Planetary Data System, EAR-A-COMPIL-5-BINMP-V5.0
- Kokubo, E., & S. Ida. 1996. Icarus, 123, 180-191.
- Kokubo, E., & S. Ida. 1998. Icarus, 131, 171-178.
- Kokubo, E., K. Yoshinaga & J. Makino. 1998. MNRAS, 297, 1967-1072.
- Kominami, J.D., J. Makino & H. Daisaka 2011. PASJ, 163, 1331-1344.
- Makino, J., & S. J. Aarseth 1992. PASJ, 44, 141-151.
- Makino, J., T. Fukushima, Y. Funato & E. Kokubo. 1998. NewA, 3, Issue 7, 411-417.
- Makino, J., K. Hiraki & M. Inaba 2007. Proceeding of the 2007 ACM/IEEE conference on Supercomputing, 1-11.
- Marchis, F., J. E. Enriquez, J. P. Emery, J. Berthier, P. Descamps, F. Vachier 2011. Icarus, 213, 252-264.
- Merline, W. J., L. M. Close, C. Dumas, J. C. Shelton, F. Menard, C. R. Chapman, D. C. Slater 2000. American Astronomical Society, DPS Meeting No.32, No13.06; Bulletin of the American Astronomical Society, Vol. 32, p.1017.
- Nakazawa K. & S. Ida 1988. Prog.Theory.Phys.Suppl., 96, 167-174.
- Nesvorný, D., A. N. Youdin & D. C. Richardson 2010. AJ, 140, 785-793.
- Noll, K. S., W. M. Grundy, E. I. Chiang, J.-L. Margot & S. D. Kern, 2008a. University of Arizona Press, pp. 345-363.
- Noll, K. S., W. M. Grundy, D. C. Stephens, H. F. Levison & S. D. Kern 2008b. Icarus, 194, 758-768.
- Pravec, P. et al. 2006. Icarus, 181, 63-93.
- Stephens, D.C. & K. S. Noll 2006. Astron. J., 131, 1142-1148.
- Walsh, K. J. & D. C. Richardson 2006. Icarus, 180, 201-216.
- Walsh, K. J., D. C. Richardson & P. Michel 2008. Nature, Volume 454, Issue 7201, pp. 188-191.
- Walsh, K. J., D. C. Richardson & P. Michel 2012. Icarus, 220, 514-529.
- Weidenschilling S.J. 2002. Icarus, 160, 212-215.

Table 1
Model List

Run	n_{init}	η	$a_{\text{min}}, a_{\text{max}}$ (AU)	n_{b}	$n_{\text{b}}/n_{\text{init}}$ (%)	$n_{\text{col,b}}$	$n_{\text{col,total}}$
S30e0.05	38283	0.05	30,30.2	72	0.19	103	243
S30e0.10	38283	0.10	30,30.2	13	0.034	71	149
S30e0.20	38283	0.20	30,30.2	9	0.024	26	66
S30e0.40	38283	0.40	30,30.2	6	0.016	11	28
S10e0.05	22000	0.05	10,10.067	4	0.018	63	283
S10e0.10	22000	0.10	10,10.067	5	0.023	26	197
S10e0.20	22000	0.20	10,10.067	1	0.0045	19	137
S10e0.40	22000	0.40	10,10.067	0	0	4	58
S3e0.05	11927	0.05	3,3.02	1	0.0084	92	450
S3e0.10	11927	0.10	3,3.02	0	0	23	324
S3e0.20	11927	0.20	3,3.02	1	0.0084	9	266
S3e0.40	11927	0.40	3,3.02	0	0	7	222
S1e0.05	1713	0.05	1,1.0067	0	0	20	141
S1e0.10	1713	0.10	1,1.0067	0	0	8	114
S1e0.20	1713	0.20	1,1.0067	0	0	4	97
S1e0.40	1713	0.40	1,1.0067	0	0	0	84

Table 1. Table of model list. n_{init} is the initial number of planetesimals. Second column η is the initial random velocity factor which is explained in section 2. a_{min} and a_{max} is the minimum value and maximum value of initial disk. n_{b} is the number of binaries after 10^4 years. The percentage expression of the starting population is the next column. $n_{\text{col,b}}$ is the number of binary-induced collisions during the simulation. $n_{\text{col,total}}$ is the total number of collision.

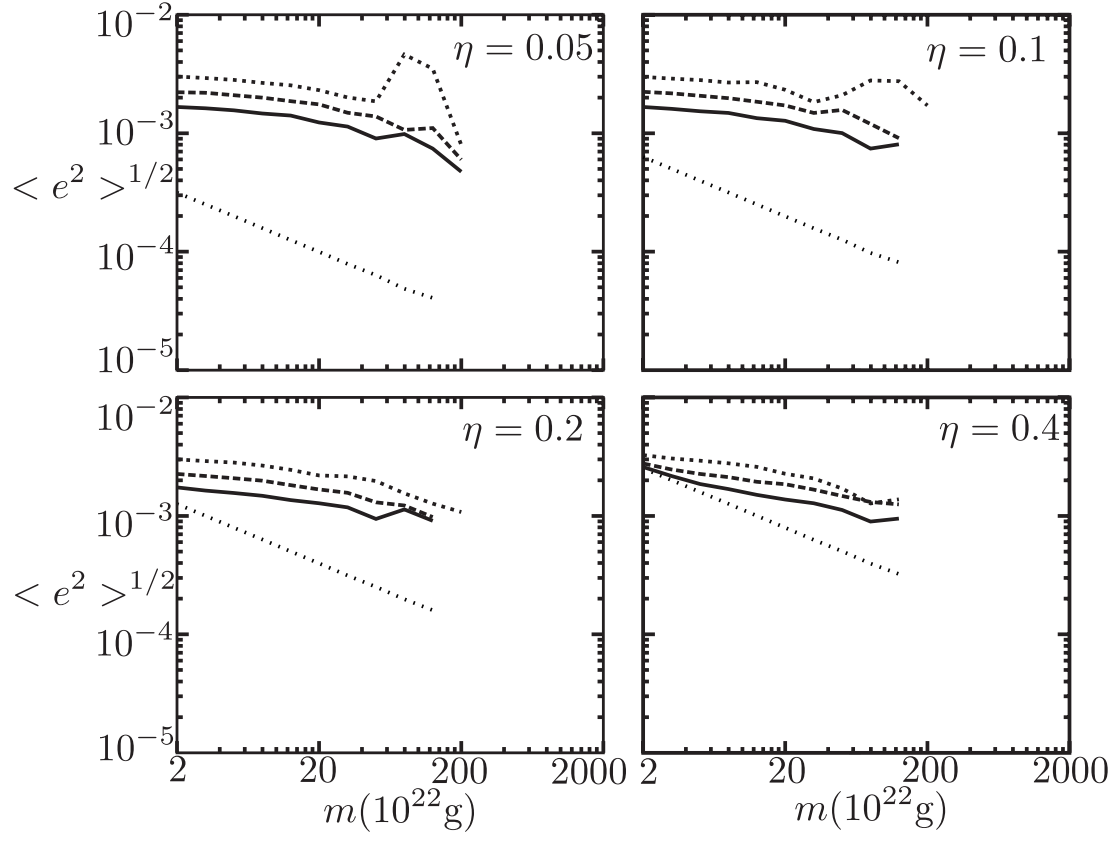


Fig. 1. RMS eccentricity plotted as a function of mass for runs S30e0.05, S30e0.10, S30e0.20 and S30e0.40. The solid line is for 1000 years, the long dashed line is for 3000 years, the short dashed line is for 10^4 years and the dotted line is for the value of initial condition, respectively.

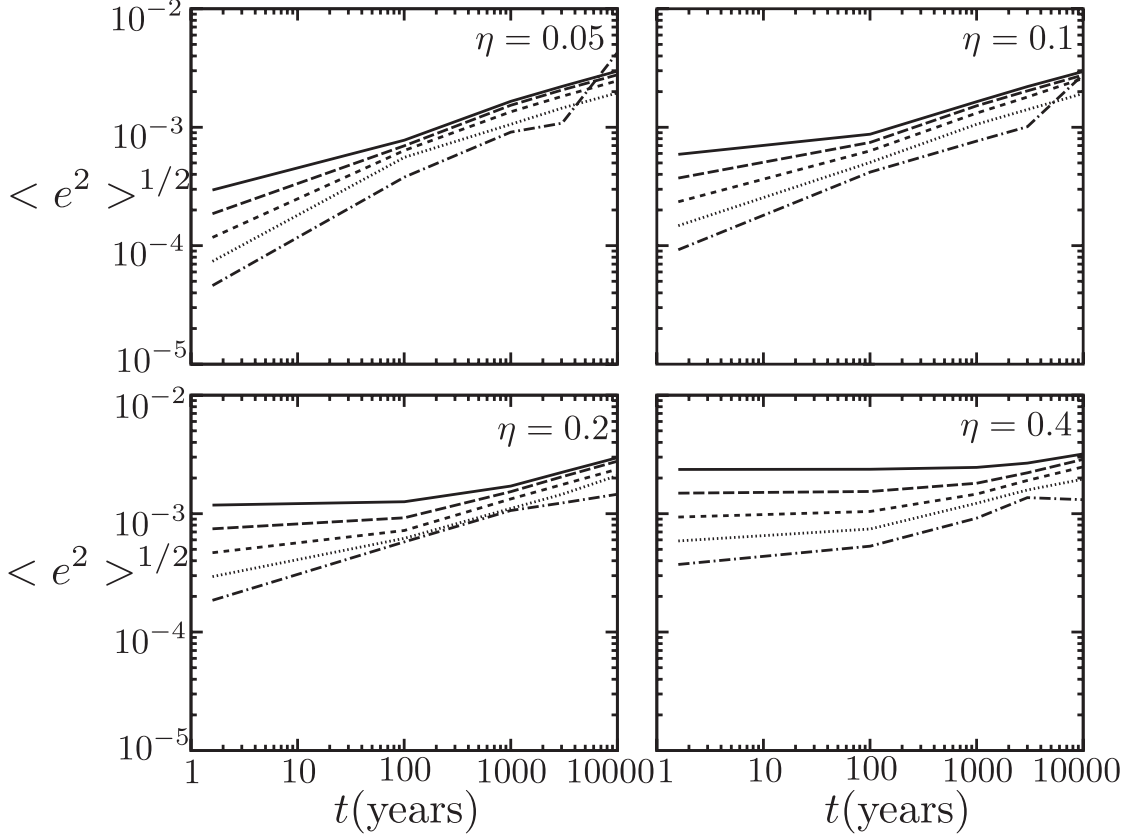


Fig. 2. Time evolution of the RMS eccentricity in five mass bins. Solid curve corresponds to the mass range $2.0 \times 10^{22} \text{g} - 5.0 \times 10^{22} \text{g}$, long dashed curve corresponds to the mass range $5.0 \times 10^{22} \text{g} - 1.26 \times 10^{23} \text{g}$, short dashed curve corresponds to the mass range $1.26 \times 10^{23} \text{g} - 3.17 \times 10^{23} \text{g}$, dotted curve corresponds to the mass range $3.17 \times 10^{23} \text{g} - 7.96 \times 10^{23} \text{g}$, and dot-dashed curve corresponds to the mass range $7.96 \times 10^{23} \text{g} - 2.0 \times 10^{24} \text{g}$, respectively. The results are for runs S30e0.05, S30e0.10, S30e0.20 and S30e0.40.

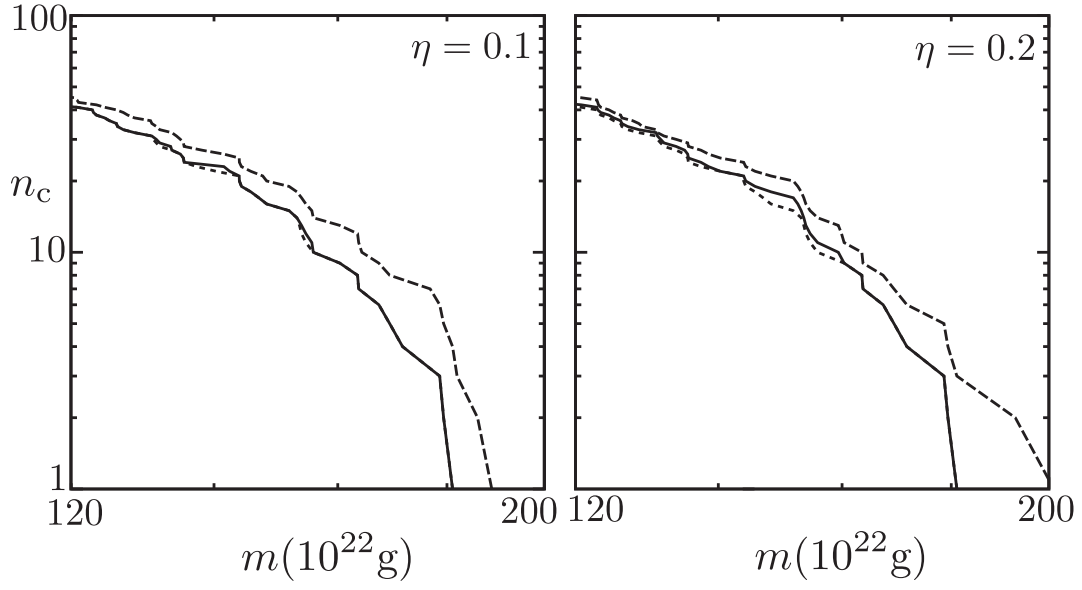


Fig. 3. Cumulative mass distribution of planetesimals of runs S30e0.10 and S30e0.20. Solid, long dashed and short dashed curves show the distributions at $t = 10^3, 10^4$ years, and the initial mass distribution, respectively.

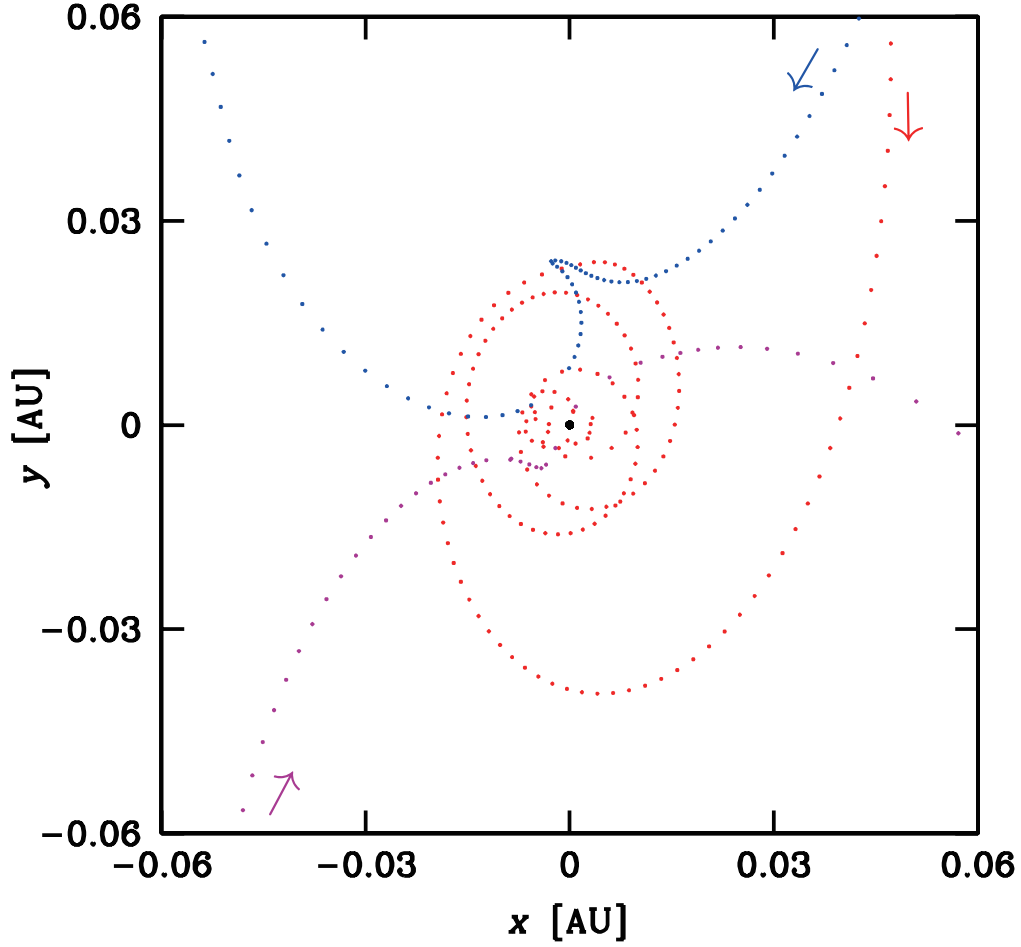


Fig. 4. Trajectories of three planetesimals during a binary formation event. Origin is placed at position of one of the final binary components (black dot). Each dot is plotted in rotational frame around the black one. First, the planetesimal colored in blue encounters the planetesimal colored in red. It makes the red planetesimal temporally bound to the black planetesimal. Then the magenta planetesimal approaches the red planetesimal taking away energy enough to make the red planetesimal bound stably.

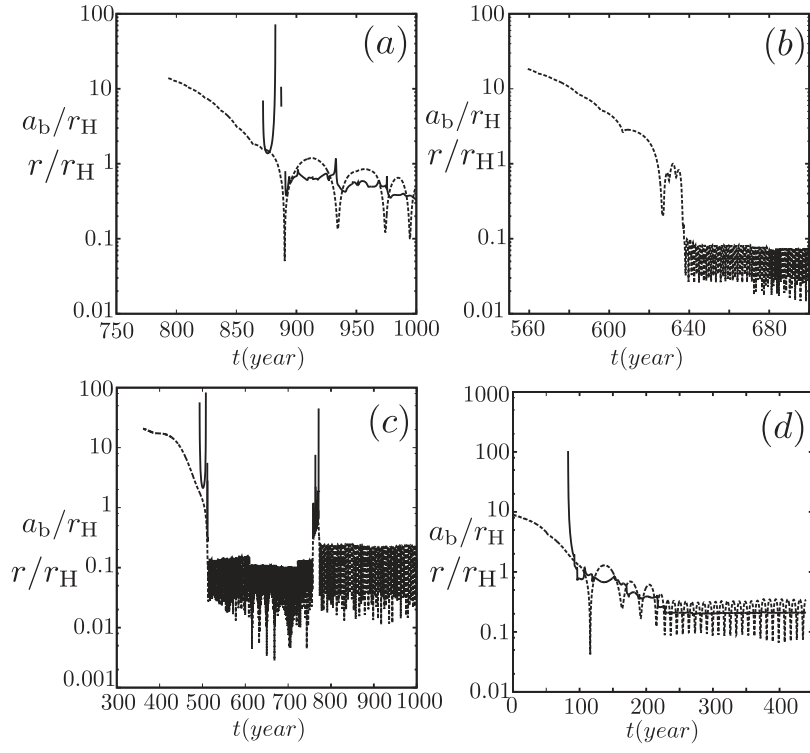


Fig. 5. The time evolution of the semi major axis a_b and separation r of two components of a binary in unit of the Hill radius r_H . The solid and dashed curves indicate a_b and r .

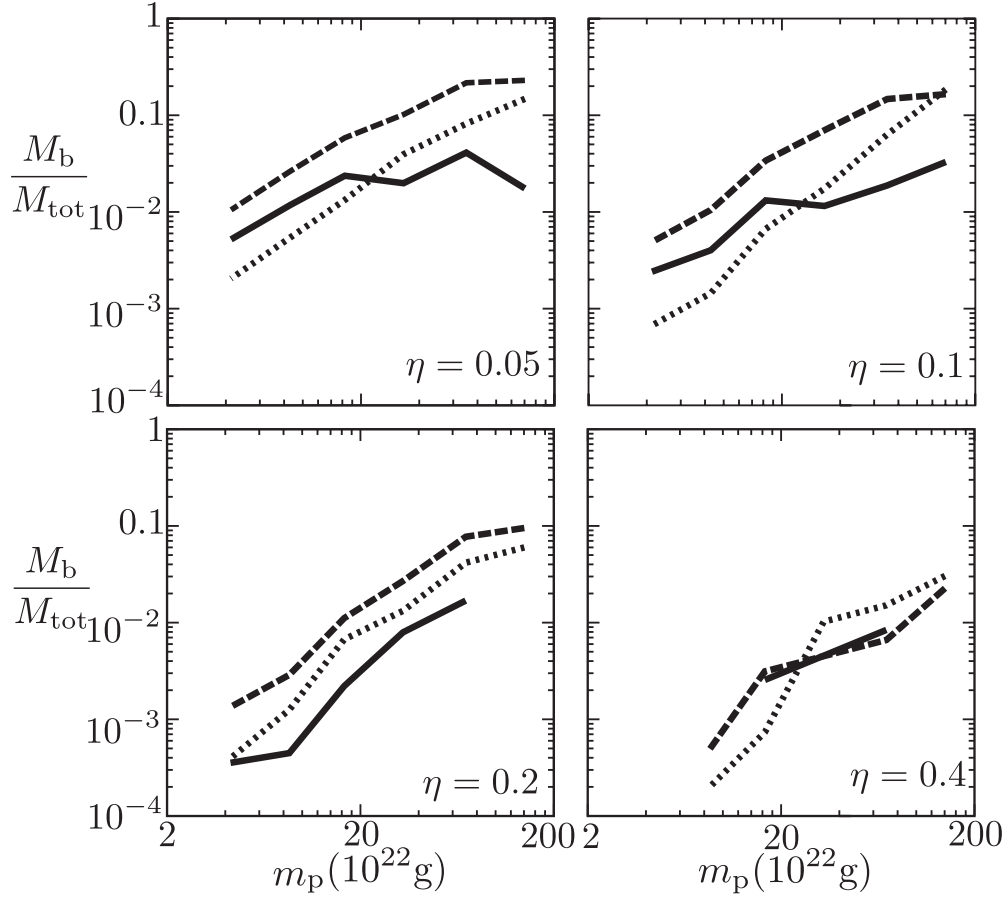


Fig. 6. Mass fraction of binaries as the function of the mass of the primary for runs S30e0.05, S30e0.10, S30e0.20 and S30e0.40. Solid, long dashed and short dashed curves corresponds to $t = 10^2, 10^3$ and 10^4 years, respectively.

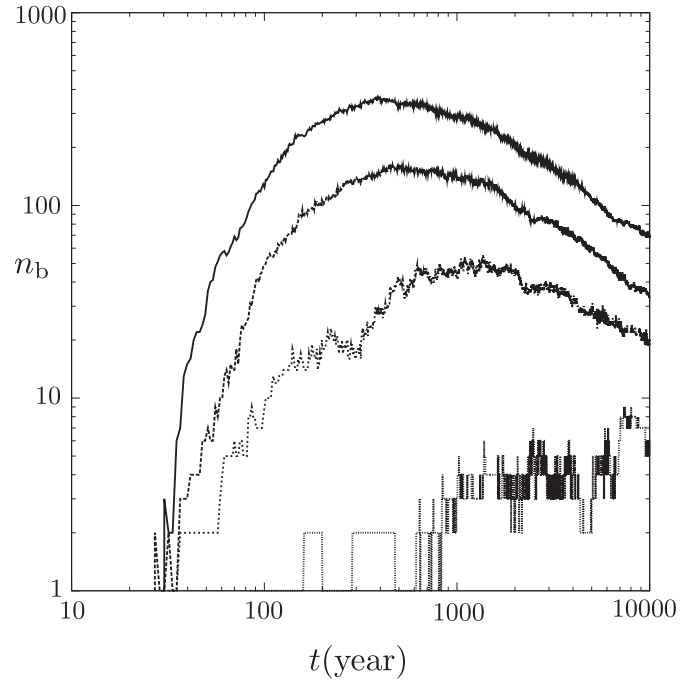


Fig. 7. Time evolution of number of binaries for runs S30e0.05(Solid), S30e0.10 (long dashed), S30e0.20 (short dashed) and S30e0.40 (dotted).

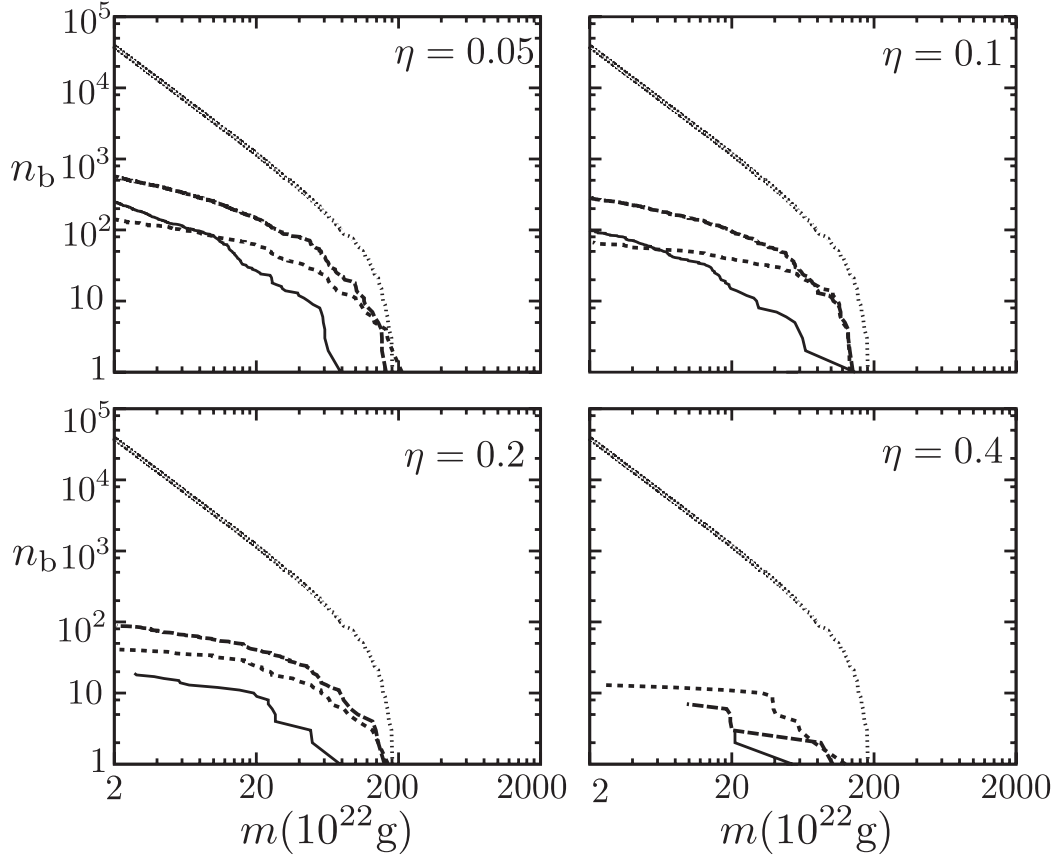


Fig. 8. Cumulative mass distribution of the binary components for runs S30e0.05, S30e0.10, S30e0.20 and S30e0.40. Both components are counted. Solid, long dashed, short dashed and dotted curves show the distributions at $t = 10^2, 10^3, 10^4$ years, and the initial mass distribution, respectively.

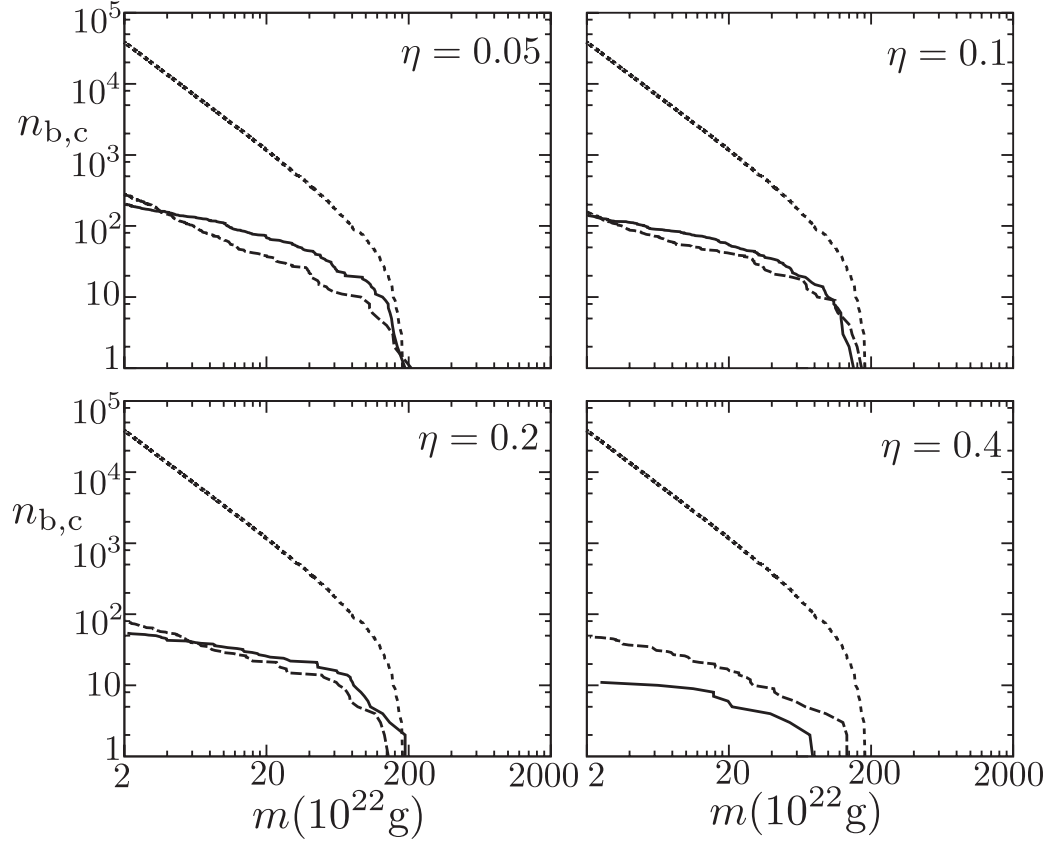


Fig. 9. Cumulative mass distribution of planetesimals that experienced binary induced collision(solid curve) and non-binary-induced ordinary collision(long dashed curve) for runs S30e0.05, S30e0.10, S30e0.20 and S30e0.40. Initial mass distribution is shown for comparison in short dashed curve

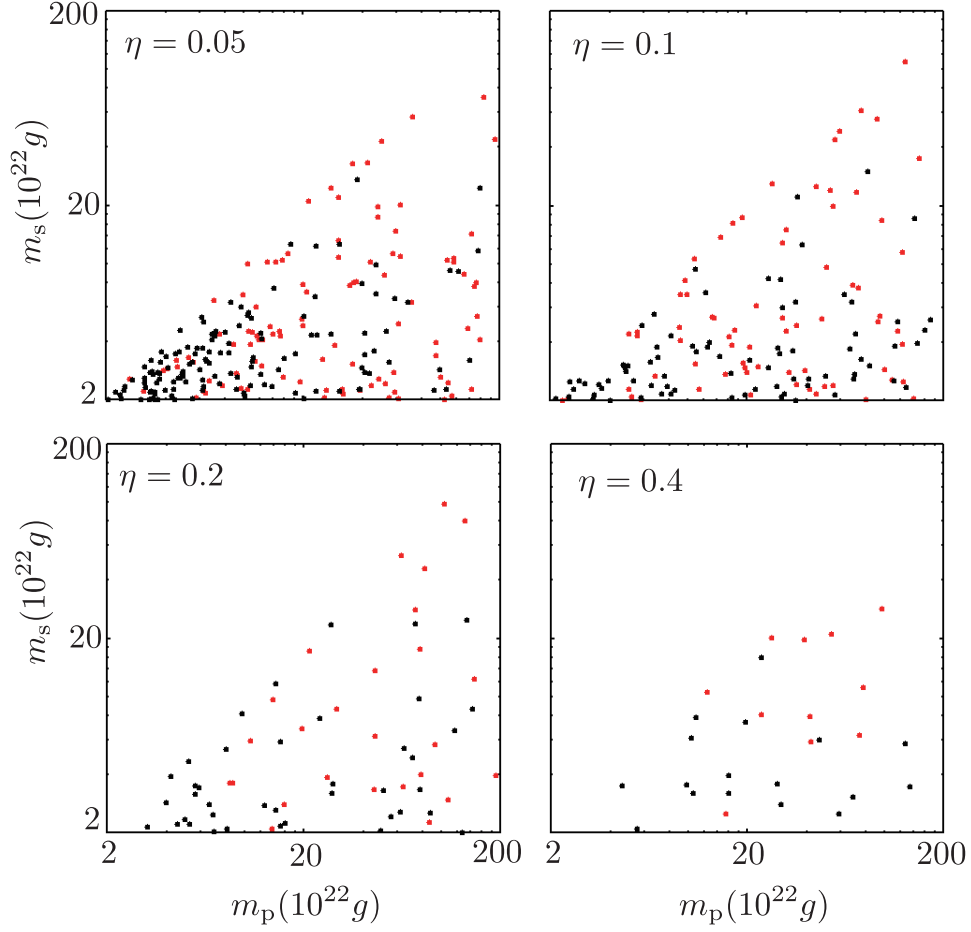


Fig. 10. Primary mass (m_p) and secondary mass (m_s) of all collisions for runs S30e0.05, S30e0.10, S30e0.20 and S30e0.40. Binary induced collisions are plotted in red and non-binary-induced collisions in black.

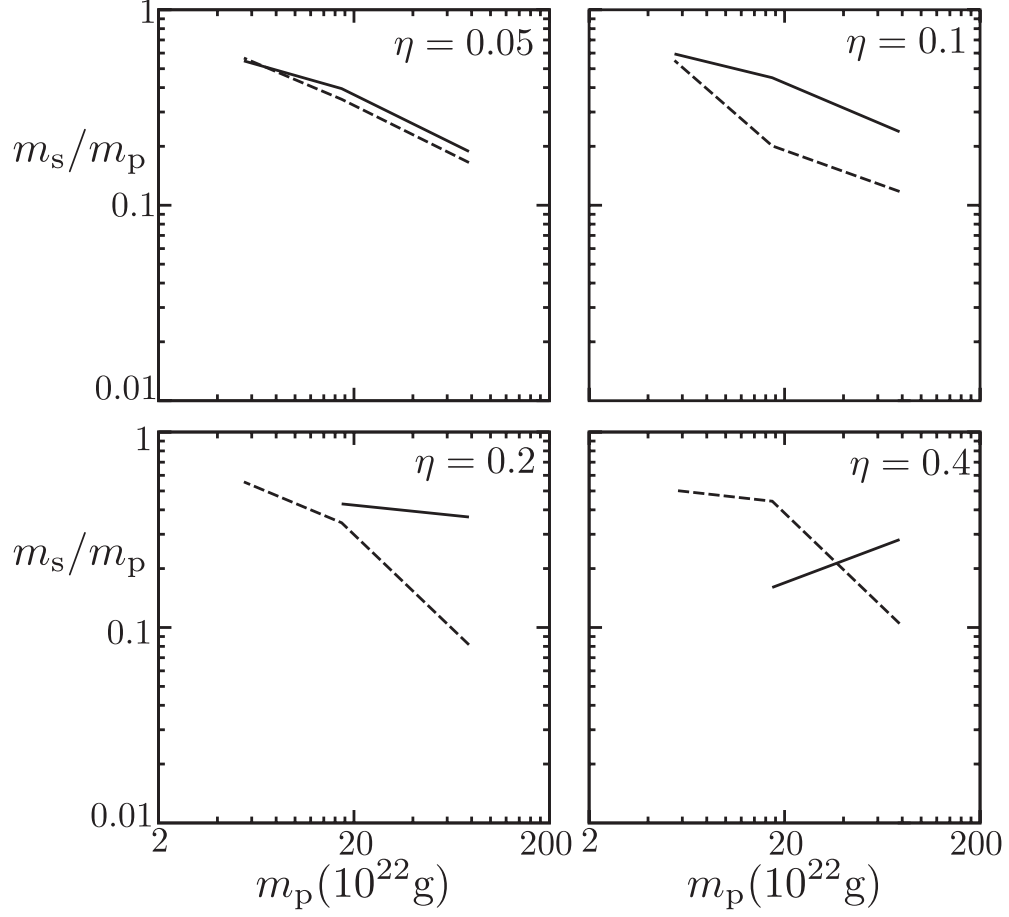


Fig. 11. Mass ratio m_s/m_p of binary-induced collisions(solid line) and of non-binary-induced collisions(long dashed line) as a function of primary mass m_p for runs S30e0.05, S30e0.10, S30e0.20 and S30e0.40.

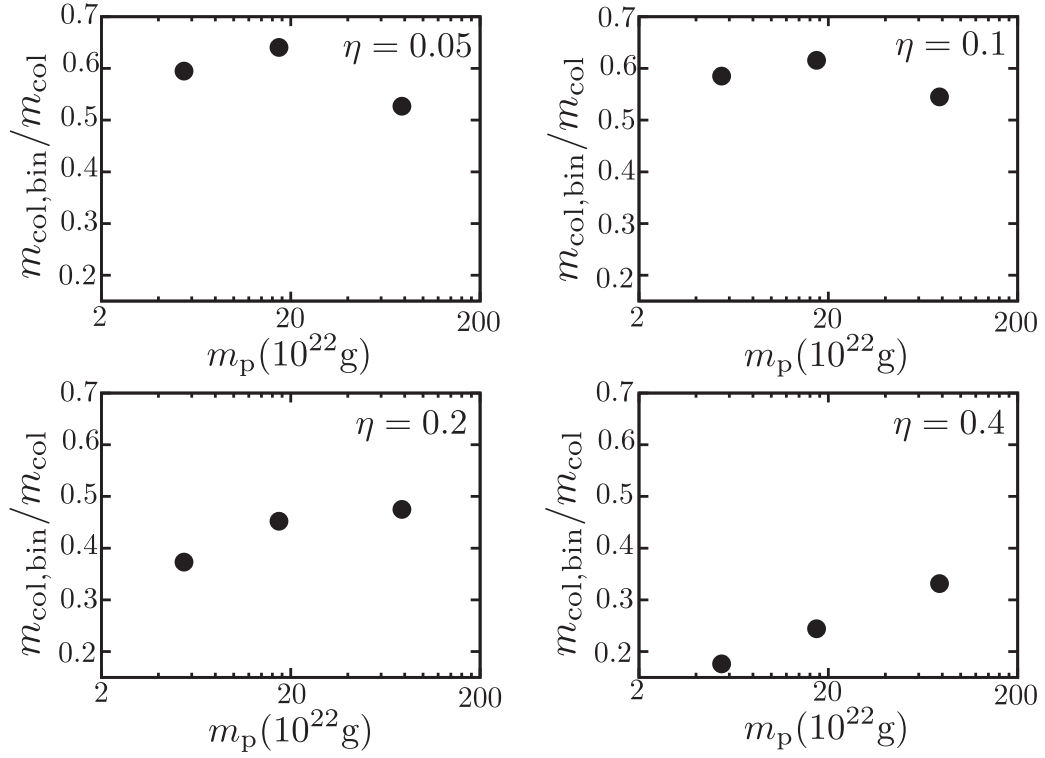


Fig. 12. The total mass of binary-induced colliding pairs normalized by total mass of planetesimals experienced collision, plotted as a function of the primary mass. The results are from runs S30e0.05, S30e0.1, S30e0.2 and S30e0.4.

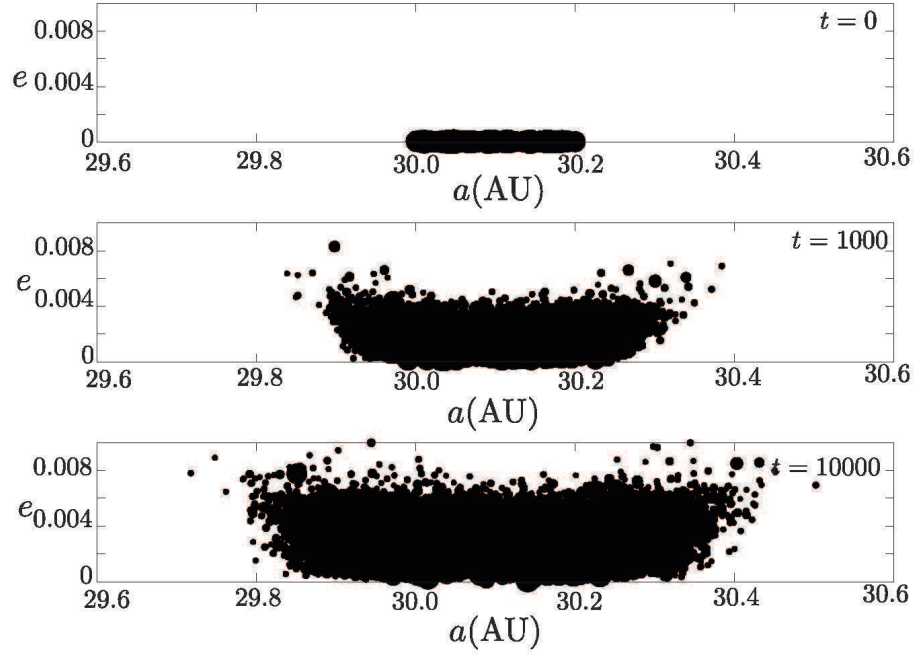


Fig. 13. Distribution of planetesimals in the plane of semi-major axis and the eccentricity. Top, middle and bottom panels show the distribution at $t = 0, 1000$ and 10000 years, respectively. The radius of the particles corresponds to the size of the planetesimals. The initial model is S30e0.05.

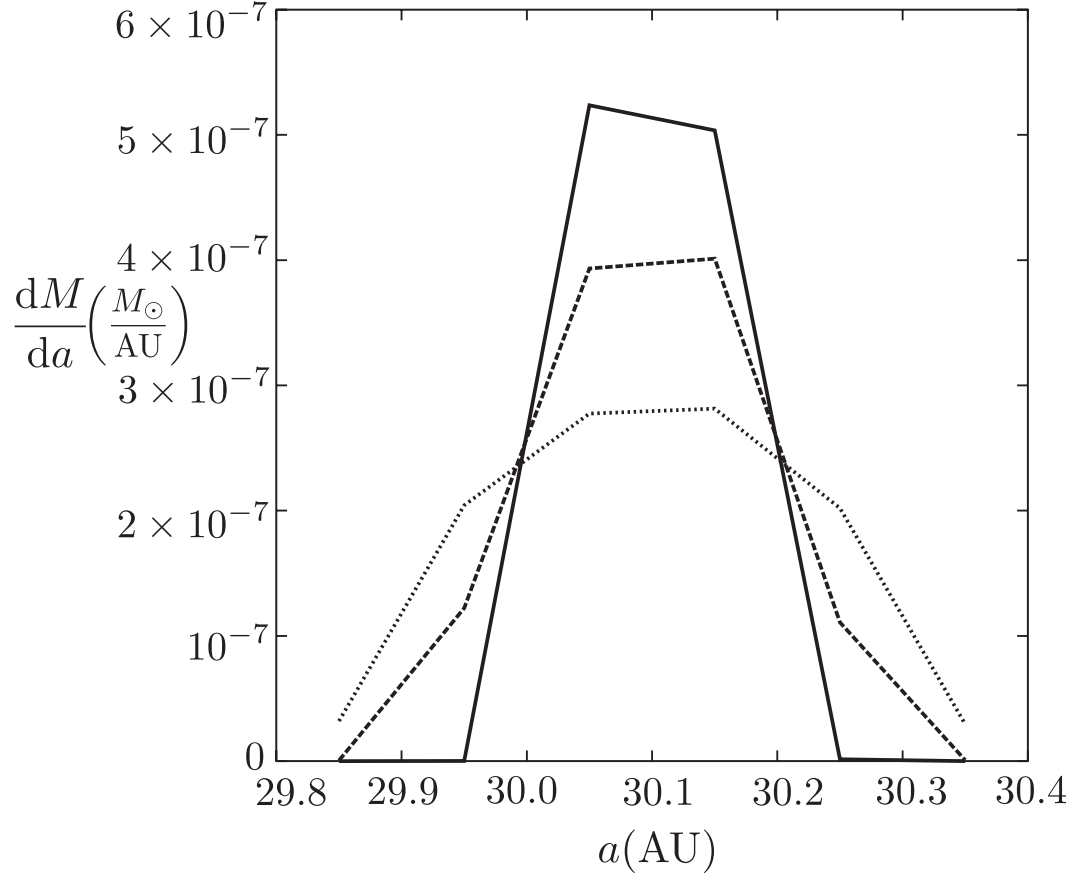


Fig. 14. Planetesimal disk surface density $dM/da(M_{\odot}/\text{AU})$ as function of semi major axis. The solid line is for $t=0$ years, dashed line is for $t=1000$ years and the dotted line is for $t=10000$ years in S30e0.05.